PERGAMON

International Journal of Heat and Mass Transfer 46 (2003) 161–173

International Journal of HEAT and MASS TRANSFER

www.elsevier.com/locate/ijhmt

Predicting turbulence and heat transfer in 3-D curved ducts by near-wall second moment closures

Kazuhiko Suga *

Combustion and Fluids Laboratory, Toyota Central R&D Labs., Inc., Nagakute, Aichi 480-1192, Japan

Received 14 December 2001; received in revised form 15 March 2002

Abstract

This paper presents discussions on predicting turbulence and heat transfer in two types of square sectioned U-bend duct flows with mild and strong curvature by recent second moment closures. Batten et al.'s [AIAA J. 37 (1999) 785] modified version of Craft and Launder's [Int. J. Heat Fluid Flow 17 (1996) 245] two-component-limit (TCL) turbulence model and Shima's [Int. J. Heat Fluid Flow 19 (1998) 549] wall-reflection free model are presently focused on. They are low-Reynolds-number models totally free from geometrical parameters. The former model is realizable and called the TCL model. For turbulent heat flux, a higher order version of the generalized gradient diffusion hypothesis by Suga and Abe [Int. J. Heat Fluid Flow 21 (2000) 37] is applied along with the TCL model. The results suggest that although both second moment closures are generally good enough for predicting flow and heat transfer in the case of mild curvature, only the realizable TCL model is reliable in the strong curvature case.

Keywords: Curved duct; Turbulence; Second moment closure; Heat flux model

1. Introduction

Turbulent heat and fluid flow through a passage with curvature has been one of the primary interests in the thermo-fluids engineering, particularly, associated with heat exchangers and turbomachinery blading. Owing to the curvature, pressure induced secondary motions produce significant consequences in the turbulent strain field and thus the level of heat transfer. To investigate this kind of turbulent flow, Chang et al. [1] first measured the detailed turbulence structure in a square sectioned U-bend duct flow with a mild curvature ratio: $R_c/D = 3.357$. The heat transfer characteristics in the same geometry were measured by Johnson and Launder [2] along with the flow field. These research works revealed the existence of "camel back" shapes in the streamwise mean velocity distribution of the curvature section. They reported that those characteristic profiles were results of strong secondary flow motions. With a strong curvature ratio, the flow along the convex wall becomes unstable and separates forming a complicated recirculating flow region. Cheah et al. [3] measured the turbulence structure in flows with such a strong curvature ratio: $R_c/D = 0.65$. This geometry is the same as that of the heat transfer experiments by Davenport [4].

In order to predict such flow and thermal structure, many numerical studies have been reported ([5–7], etc). In the recent review of Iacovides and Launder [8], well covering major numerical results, they concluded that a low Reynolds number (LRN) model was far more reliable than bridging the wall functions. They also recommended the use of a second moment closure (SMC) to predict duct flows despite the problems of wall-reflection terms in modelling the pressure–strain correlation. (It had been difficult to eliminate geometry oriented parameters from the wall-reflection terms even though such a parameter was hard to be determined in complicated flow geometry.)

According to the recent progress in turbulence modelling, we now have several more advanced LRN SMCs such as the models proposed by Launder and Tselepidakis [9], Hanjalić and Jakirlić [10], Craft and

* Tel.: +81-561-63-4439; fax: +81-561-63-6114.
E-mail address: k-suga@mosk.tytlabs.co.jp (K. Suga).

0017-9310/03/$ - see front matter
PII: S0017-9310(02)00249-1

Nomenclature

a_{ij}	anisotropic stress, $(\overline{u_iu_j}/k - 2/3\delta_{ij})$	S_{ij}	strain tensor, $(\partial U_i/\partial x_j + \partial U_j/\partial x_i)$
A	Lumley's stress flatness parameter, $(1 - (9/8)(A_2 - A_3))$	U_i	mean velocity component
		$\overline{u_iu_j}$	Reynolds stress
A_2	$a_{ij}a_{ij}$	U_b	bulk mean velocity
A_3	$a_{ij}a_{jk}a_{ki}$	$\overline{u_i\theta}$	turbulent heat flux
d_{ij}	diffusion term of Reynolds stress	ε	dissipation rate of k
D	duct height	ε_{ij}	dissipation rate of Reynolds stress
k	turbulence energy	$\tilde{\varepsilon}$	$\varepsilon - 2\nu(\partial\sqrt{k}/\partial x_k)(\partial\sqrt{k}/\partial x_k)$
l	turbulent length scale, $(k^{1.5}/\varepsilon)$	ϕ_{ij}	pressure-strain term of Reynolds stress
Nu	Nusselt number	Π_{ij}	pressure correlation term of Reynolds stress
P_{ij}	production term of Reynolds stress		
Pr	Prandtl number	θ	section angle or streamwise direction
R_c	bend radius	Θ	mean temperature
Re	bulk Reynolds number, $(U_\mathrm{b}D/\nu)$	ν	kinematic viscosity
R_t	turbulent Reynolds number, $(k^2/(\nu\varepsilon))$	τ, $\tilde{\tau}$	turbulent time scale, $(k/\varepsilon,\ k/\tilde{\varepsilon})$
S	$\tau\sqrt{S_{ij}S_{ij}/2}$	Ω	$\tau\sqrt{\Omega_{ij}\Omega_{ij}/2}$
S_I	$S_{ij}S_{jk}S_{ki}/(S_{ln}S_{ln})^{3/2}$	Ω_{ij}	vorticity tensor, $(\partial U_i/\partial x_j - \partial U_j/\partial x_i)$

Launder [11] (the CL model), and Shima [12]. Amongst them, the CL and the Shima models were designed to be totally free from topographical parameters such as wall normal distance and a wall normal vector. For industrial applications, elimination of those parameters is very much preferred because of the complexity of the flow geometry.

To establish a full realizable LRN SMC, the UMIST group has been developing a series of models [9,11,13] based on the most general "cubic" quasi-isotropic (QI) model for the pressure–strain term initially proposed by Fu [14]. Those models have been developed considering realizability of Reynolds stresses in two-component-limit (TCL) turbulence which appear near wall and free surface boundaries so that they are called the TCL SMCs. One of the latest versions is the one by Batten et al. [15]. They extended the applicability of the CL model to compressible flows by adding some minor changes and thus their version was called the modified CL model.

On the other hand, the Shima model is based on the much simpler quasi-linear model for the pressure–strain term and it was well calibrated in flows near curved walls [16]. As Shima himself admitted in the paper [12], it was developed without considering full realizability. However, since the model works generally well in many flows, it is certainly useful for engineering CFD despite its theoretical flaws.

Although solving every component of the Reynolds stress tensor requires more computational resources than applying an eddy viscosity model (EVM), SMCs are thought to be more general approach. In a cylindrical coordinate system, for example, it is well known that curvature related terms are retained in the transport equations of SMCs but not in those of EVMs. This implies that the intrinsic curvature effects are in SMCs without any special consideration for them. It is thus useful for industrial engineers to provide the extensive validation of the SMCs if there is no difficulty to apply them for complicated flow fields. Since the modified CL and the Shima models are LRN SMCs free from topographical parameters, they are easy to be applied for any geometry, in principle. Thus, the performance of these two models is of interest to the industrial CFD engineers.

For the thermal field computation, the generalized gradient diffusion hypothesis (GGDH) of Daly and Harlow [17] is usually used to describe turbulent heat flux in the context of SMCs. However, it is well known that one cannot predict the streamwise heat flux component reasonably well with it [18]. Although the streamwise component is unimportant for predicting the thermal field in a fully developed flow parallel to a wall, it does not necessarily mean that the streamwise component is always unimportant.

Hence, there have been several proposals of new turbulent heat flux models which have better accuracy even for the streamwise component (e.g., [19,20]). Amongst them, the model of Suga and Abe [21] has a generally expanded form of the GGDH model with introduction of higher order terms. This higher order GGDH (HOGGDH) model was constructed in combination with nonlinear EVMs. However, since a GGDH-type of heat flux model heavily relies on the predicted turbulence anisotropy, it is reasonably expected that coupling it with a SMC is more suitable to predict complex thermal fields.

Therefore, in order to update the information for computing the flow and heat transfer in curved ducts, this paper discusses the results by the modified CL and the Shima SMCs in the square sectioned U-bend ducts with the mild and strong curvature ratios ($R_c/D = 3.357$, 0.65). The standard GGDH and the HOGGDH heat flux models are coupled with those SMCs for turbulent heat transfer. According to the fact that the GGDH-type of heat flux model depends on the predicted stress behaviour, minor modifications on the model coefficients or functions of both flow and heat flux models have been occasionally tried to achieve their full potential.

2. Turbulence models

In this paper, the full set of equations and coefficients involved in the models are not described in detail unless modifications are made in the present study. See the original papers referred to for the details if necessary.

2.1. Flow field

2.1.1. Second moment closures

The transport equation of the Reynolds stress is

$$\frac{D\overline{u_iu_j}}{Dt} = d_{ij} + P_{ij} + \Pi_{ij} - \varepsilon_{ij}. \tag{1}$$

The pressure correlation, Π_{ij}, is usually split into the pressure–diffusion and the pressure–strain, ϕ_{ij}, terms. Whilst the former part is included in the turbulent diffusion term in the traditional way of modelling, the latter part is the "core" term to be focused on. Therefore, there have been many proposals for ϕ_{ij} (e.g., [22,23]). However, in the wall-reflection terms, which correspond to the surface integrals of the pressure fluctuation, topographical parameters such as a wall normal vector and the distance from a wall have been usually used (e.g., [10,24,25]). Since those geometry oriented terms are not preferable for complicated flow applications, Craft and Launder [11] and Shima [12] developed LRN SMCs eliminating such wall-reflection terms.

The Shima model is based on the rather simple quasi-linear model:

$$-\varepsilon_{ij} + \phi_{ij} = -2/3\delta_{ij}\varepsilon + \phi_{ij1} + \phi_{ij2}, \tag{2}$$

$$\phi_{ij1} = -c_1\varepsilon a_{ij}, \tag{3}$$

$$\phi_{ij2} = -c_2\left(P_{ij} - 1/3\delta_{ij}P_{kk}\right) - c_3\left(D_{ij} - 1/3\delta_{ij}D_{kk}\right) - c_4kS_{ij}, \tag{4}$$

where $P_{ij} = -(\overline{u_iu_k}\partial U_j/\partial x_k + \overline{u_ju_k}\partial U_i/\partial x_k)$, $D_{ij} = -(\overline{u_iu_k} \times \partial U_k/\partial x_j + \overline{u_ju_k}\partial U_k/\partial x_i)$. The terms ϕ_{ij1} and ϕ_{ij2} are the slow re-distribution part and the rapid re-distribution part of ϕ_{ij}, respectively. For the coefficients, Shima introduced functional forms including Lumley's [26] stress flatness parameter, A, to apply the above model for near-wall turbulence. Owing to vanishing of A in two-component turbulence limits, A has been used to detect near-wall turbulence in many LRN SMCs [9,10,25]. The Shima model was successfully evaluated in many 2-D flows near-curved walls [16]. However, the coefficients, c_1–c_4, of the Shima model do not satisfy the requirement for Green's condition set forth by Launder et al. [22] and thus the model is unrealizable as admitted by Shima himself [12]. Therefore, any inconsistency with theoretical behaviour of quantities (particularly, near a wall) should be tolerated when the model is applied. (See Shima [12] for the details of the model.)

Craft and Launder [11] employed a much more complicated pressure–strain model after a series of development for a full realizable TCL SMC by the UMIST group [9,13]. The employed pressure–strain model is the cubic QI model of Fu [14]. The CL model is the first LRN version of its series totally free from topographical parameters. Its re-distributive term was modelled as

$$\phi_{ij} = \phi_{ij1} + \phi_{ij2} + \phi_{ij1}^{\mathrm{inh}} + \phi_{ij2}^{\mathrm{inh}}, \tag{5}$$

where $\phi_{ij1}^{\mathrm{inh}}$, $\phi_{ij2}^{\mathrm{inh}}$ are the correction terms for inhomogeneity effects. The cubic QI pressure–strain model employs the most general forms for ϕ_{ij1} and ϕ_{ij2} as

$$\phi_{ij1} = -c_1\tilde{\varepsilon}\left\{a_{ij} + c_1'\left(a_{ik}a_{jk} - \frac{1}{3}A_2\delta_{ij}\right)\right\} - c_1''\tilde{\varepsilon}a_{ij}, \tag{6}$$

$$\begin{aligned}\phi_{ij2} = {} & -0.6\left(P_{ij} - \frac{1}{3}P_{kk}\delta_{ij}\right) + 0.3a_{ij}P_{kk} \\ & - 0.2\left\{\frac{\overline{u_ju_k}\,\overline{u_iu_l}}{k}S_{kl} - \frac{\overline{u_ku_l}}{k}\left(\overline{u_iu_k}\frac{\partial U_j}{\partial x_l} + \overline{u_ju_k}\frac{\partial U_i}{\partial x_l}\right)\right\} \\ & - c_2\left\{A_2\left(P_{ij} - D_{ij}\right) + 3a_{mi}a_{nj}(P_{mn} - D_{mn})\right\} \\ & + c_2'\left[\left(\frac{7}{15} - \frac{A_2}{4}\right)\left(P_{ij} - \frac{1}{3}\delta_{ij}P_{kk}\right)\right. \\ & \quad + 0.1\left\{a_{ij} - \frac{1}{2}\left(a_{ik}a_{kj} - \frac{1}{3}\delta_{ij}A_2\right)\right\}P_{kk} \\ & \quad - 0.05a_{ij}a_{kl}P_{kl} + 0.1\left\{\left(\frac{\overline{u_iu_m}}{k}P_{jm} + \frac{\overline{u_ju_m}}{k}P_{im}\right)\right. \\ & \quad\quad \left. - \frac{2}{3}\delta_{ij}\frac{\overline{u_lu_m}}{k}P_{lm}\right\} + 0.1\left(\frac{\overline{u_iu_l}\,\overline{u_ju_k}}{k^2}\right. \\ & \quad\quad \left.\left. - \frac{1}{3}\delta_{ij}\frac{\overline{u_lu_m}\,\overline{u_ku_m}}{k^2}\right)(6D_{kl} + 13kS_{kl}) \right. \\ & \quad \left. + 0.2\frac{\overline{u_iu_l}\,\overline{u_ju_k}}{k^2}(D_{kl} - P_{kl})\right].\end{aligned} \tag{7}$$

The inhomogeneity correction terms, $\phi_{ij1}^{\mathrm{inh}}$, $\phi_{ij2}^{\mathrm{inh}}$, effectively replaced the traditional wall-reflection terms defining inhomogeneity indicators which were basically the gradients of turbulent length scales. This CL model is realizable and validated in TCL turbulence boundaries

[11]. Even though the model equations are very complicated, it is thought to be rather economical because the realizability contributes to rapid convergence of the solution.

Recently, Batten et al. [15] of the UMIST group modified the CL model and extended its applicability to compressible flows. The present study thus broadly follows this modified version yet with some minor re-tuning in the model functions. It is made to comply with the theoretical near-wall behaviour of turbulence quantities: A and ε_{22} which has been found to be particularly crucial in the HOGGDH heat flux model. The equations and coefficients of the present version of the TCL model (called the TCL SMC hereafter) are summarised in the Appendix A.

2.2. Heat flux models

In complex turbulent thermal field computations, as Launder [18] noted, the GGDH model of Daly and Harlow [17]:

$$\overline{u_i\theta} = -c_\theta \tau \overline{u_i u_j} \frac{\partial \Theta}{\partial x_j}, \tag{8}$$

is reasonably successful when near-wall turbulence anisotropy is captured. It is thus normally used along with a SMC. However, it still rather under-predicts the streamwise heat flux component [18].

In order to improve the performance of the GGDH model, Suga and Abe [21] expanded the expression of the GGDH model by introducing extra terms including a quadratic product of the Reynolds stress tensor. They showed that their HOGGDH heat flux model successfully reproduced each heat flux component in channel flows at a wide range of fluid Prandtl numbers. The model form may be written as

$$\overline{u_i\theta} = -c_\theta k \tilde{\tau} (\sigma_{ij} + \alpha_{ij}) \frac{\partial \Theta}{\partial x_j}, \tag{9}$$

where the symmetric tensor σ_{ij} contains linear and quadratic terms as

$$\sigma_{ij} = c_{\sigma 1} \overline{u_i u_j}/k + c_{\sigma 2} \overline{u_i u_l}\,\overline{u_l u_j}/k^2. \tag{10}$$

Inclusion of the quadratic term (the second term on the rhs of Eq. (10)) is effective to predict the streamwise heat flux component [27]. The asymmetric tensor α_{ij} was modelled as

$$\alpha_{ij} = c_{\alpha 1} \tilde{\tau} \left(\Omega_{il} \overline{u_l u_j}/k + \Omega_{lj} \overline{u_i u_l}/k \right). \tag{11}$$

The proposed magnitude of the coefficient c_θ in the HOGGDH model was especially for the nonlinear EVMs, and thus the re-adjusted one for the SMCs is

$$c_\theta = \frac{0.4 + 0.2 \exp\{-(R_t/175)^3\}}{\left[1 - \exp\{-(A/0.05)^2\}\right]^{1/4}}. \tag{12}$$

Note that this HOGGDH model complies with the linearity and independence principles of scalar transport set forth by Pope [28]. (See [21] for the details of the other model coefficients.)

3. Results and discussions

As illustrated in Fig. 1, turbulent U-bend duct flows with two different curvature ratios ($R_c/D = 3.357$, 0.65) are discussed to assess the model performance. The computer program used is a cell vertex unstructured grid code developed by Suga et al. [29]. It uses the third-order MUSCL-type scheme for the convection terms while the second-order central difference is applied for the other terms.

The computational grids used extend up to the symmetry plane and consist of 121 (streamwise) $\times$ 81(x) $\times$ 41(y) (with 1D inlet and 3D outlet tangents) and 151 $\times$ 100 $\times$ 50 (with 3D inlet and 9D outlet tangents) nodes respectively for the cases of $R_c/D = 3.357$ and 0.65. All their first grid node points from the wall boundaries are allocated within unity of the wall unit to ensure the performance of LRN turbulence models. These computational grids presently employed are the same as those used in the previous study [29]. They had been systematically verified to be good enough for grid independent solutions.

For providing the inlet conditions, separate computations of fully developed straight duct flows have been performed. The total CPU time required for the convergence of a steady state computation by the TCL SMC has been 4–5 times as long as that of the basic LRN k–ε model. The Shima model has needed a little shorter CPU time than that of the TCL SMC though,

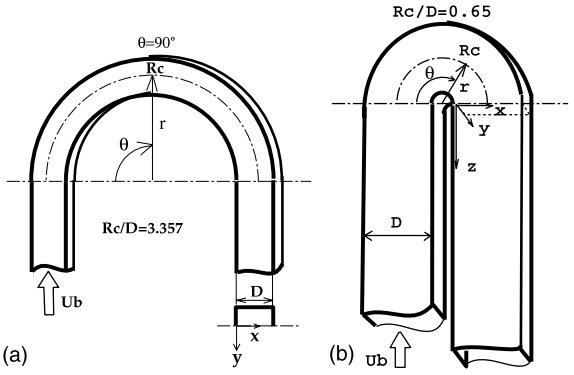

Fig. 1. Square sectioned 180° U-bend duct flows; (a) $R_c/D = 3.357$; (b): $R_c/D = 0.65$.

due to its unrealizability, some ad hoc treatments, such as removing some model terms temporarily, have been occasionally needed to stabilise the initial iterations.

3.1. U-bend duct of $R_c/D = 3.357$

The considered air flow and thermal conditions are the same as the experiments [1,2] and the bulk Reynolds number is $Re = 56700$. As in the experiments, the thermal wall boundary condition is a constant wall heat flux condition. In this case, no separating flow was observed in the experiments.

3.1.1. Flow field

Fig. 2(a)–(d) compare the predicted streamwise mean velocity distribution at the four streamwise sections of $\theta = 45°$, 90°, 130° and 177°, respectively. At each section, the velocity distribution at $2y/D = 0$, 0.25, 0.5, 0.75 is plotted. (The symmetry plane corresponds to $2y/D = 0$ while the bottom or top wall corresponds to

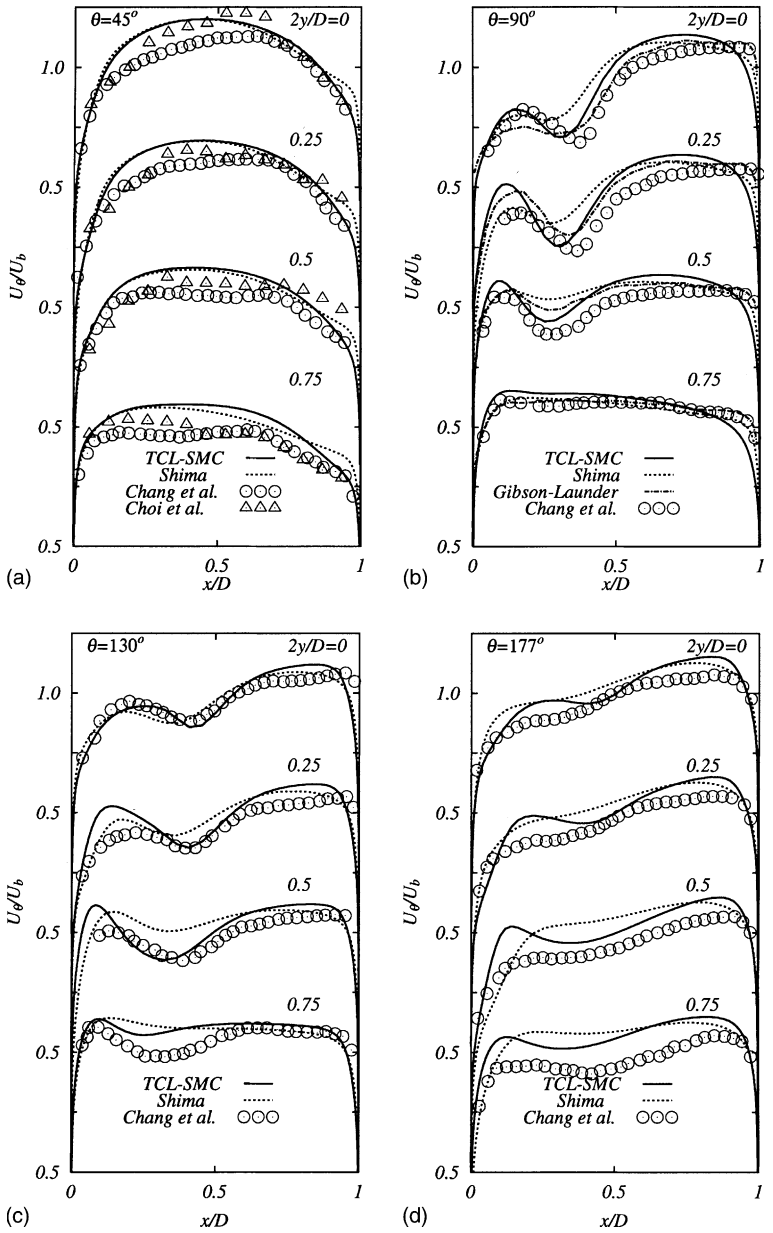

Fig. 2. Streamwise mean velocity in the U-bend duct of $R_c/D = 3.357$ at $Re = 56700$.

$2y/D = 1$.) As shown in Fig. 2(a), some discrepancies can be found between the experiments of Chang et al. [1] and Choi et al. [30] in the centre region. Choi et al. also measured the flow field of the same geometry as of Chang et al. They reported that discrepancies similar to those in Fig. 2(a) were also seen at the other sections. This implies that such a level of experimental uncertainty needs to be considered.

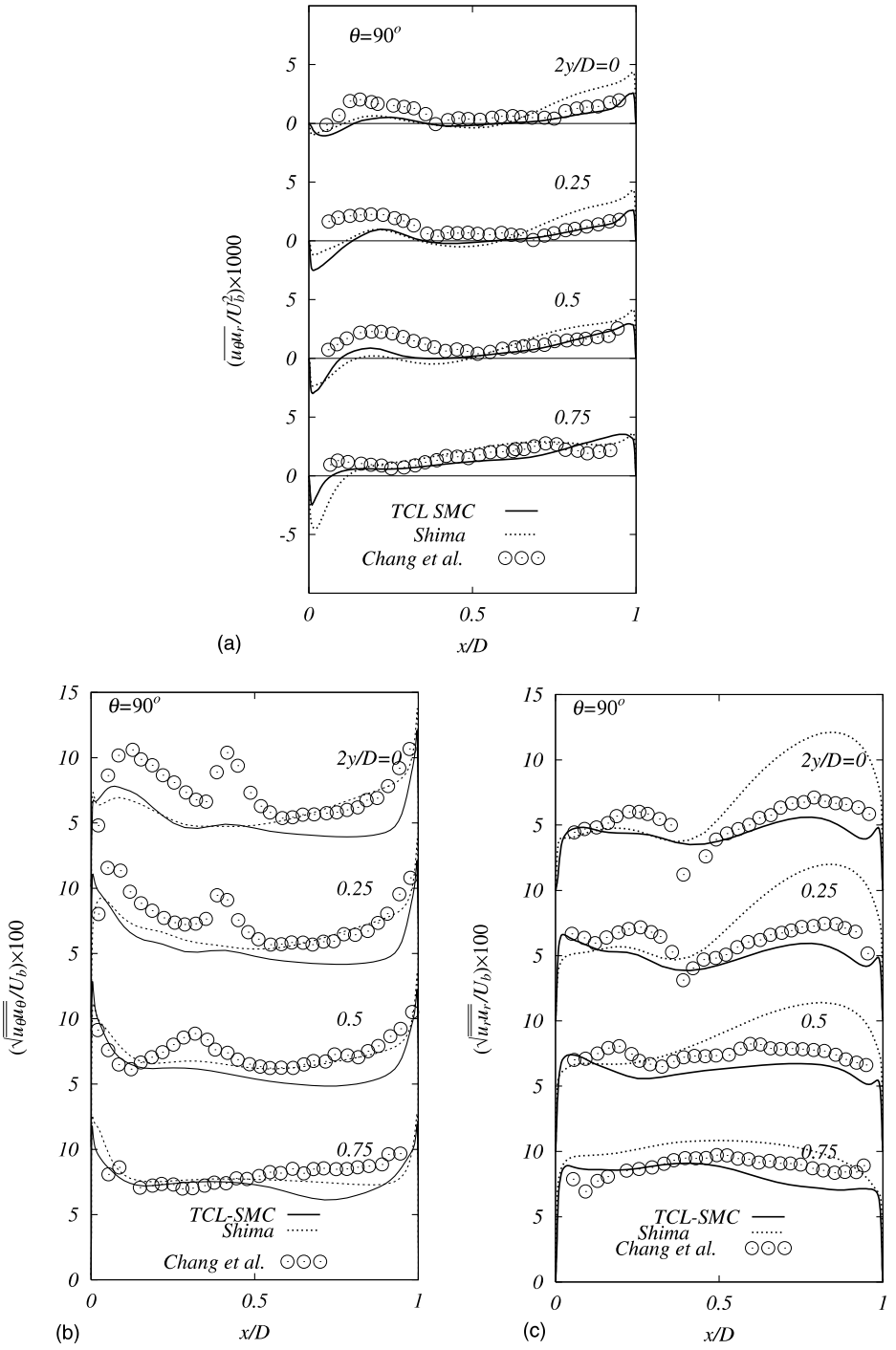

Fig. 3. Reynolds stresses in the U-bend duct of $R_c/D = 3.357$ at $\theta = 90°$.

In Fig. 2(b), the results of the Gibson–Launder model [24] produced by the earlier work of Iacovides et al. [6] are plotted. (Since the Gibson–Launder model is a high Reynolds number model, Iacovides et al. used the mixing length hypothesis for the near-wall sublayer.) It is obvious that the performance of the presently considered wall-reflection free LRN SMCs (the TCL and the Shima models) is comparable to that of the Gibson–Launder model which includes the wall-reflection terms. This confirms that the modelling without wall-reflection terms is successful in such a 3-D flow field.

Although the agreement between the predictions and the experiments is not perfect, both LRN SMCs generally reproduce well the characteristic velocity distribution of the experiments. Particularly, as shown in Fig. 2(b)–(c), the main characteristic of this flow is the appearance of the camel back shapes in the velocity distribution. These shapes are the results of loss of the streamwise momentum due to the secondary flow forming a strong downward motion from the symmetry plane to the bottom (or top) wall [2]. Both models successfully reproduce these characteristic profiles while the TCL model performs slightly better than the Shima model, particularly at the $\theta = 90°$ section.

Fig. 3(a)–(c) respectively show the distribution of the Reynolds shear stress: $\overline{u_\theta u_r}$ and the normal stresses: $\overline{u_\theta^2}$, $\overline{u_r^2}$ at the $\theta = 90°$ section. Although the predicted shear stress distribution accords with the experiments acceptably, both models fail to reproduce the experimental profiles of normal stresses correctly, particularly in the regions where the experiments show kink profiles corresponding to the dents in the mean velocity distribution. This suggests that both models still need to be improved for the stress behaviour. Furthermore, as Fig. 3(b) shows, the TCL SMC somehow under-predicts the streamwise normal stress: $\overline{u_\theta^2}$ in the outer side region $(x/D > 0.5)$ while Fig. 3(c) shows that the Shima model tends to over-predict the wall normal stress: $\overline{u_r^2}$ there. This latter predictive tendency of the Shima model affects its heat transfer prediction discussed in the next subsection. (Note that the TCL SMC's profiles of $\overline{u_\theta^2}$ correspond better with Choi et al.'s experiments, particularly at $2y/D = 0$, 0.25. This implies that the accuracy of the TCL SMC for the streamwise stress may be appropriate.)

3.1.2. Heat transfer

Before discussing the U-bend duct heat transfer, the performance of the standard GGDH (simply called the GGDH model hereafter) and the HOGGDH heat flux models is discussed. Fig. 4 compares the local *Nu* distribution of the fully developed flow in a straight square duct by the SMCs with the GGDH and the HOGGDH models. As in the DNS by Fukushima and Kasagi [31], a constant wall temperature condition is employed. The HOGGDH model is only coupled with the TCL SMC simply because the HOGGDH model cannot work with the Shima model. It seems to require significant further development to have a tailor-made version of the HOGGDH for the Shima model. The major reason is that the Shima model produces an incorrect wall value (about 0.1) of A, while it should fall to zero according to the near-wall variation $A \propto y^2$. This incorrect wall limiting behaviour results in the wrong variation of the model functions including A in the HOGGDH model.

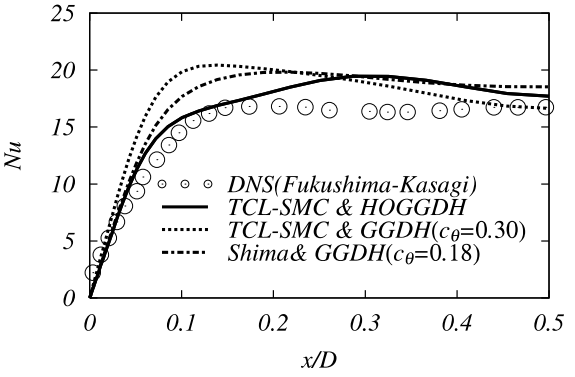

Fig. 4. Local Nusselt number distribution in the square sectioned duct at $Re = 4500$ and $Pr = 0.71$.

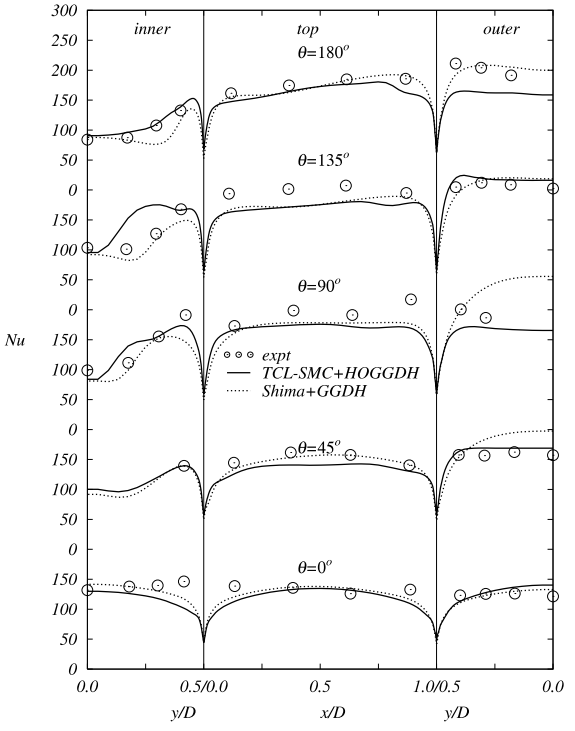

Fig. 5. Local Nusselt number distribution in the U-bend duct flow of $R_c/D = 3.357$ at $Re = 56700$ and $Pr = 0.71$; expt.: Johnson and Launder [2].

As shown in Fig. 4, the combination of the TCL SMC and the HOGGDH improves the result of the combination of the TCL SMC and the GGDH in the region near the side wall ($x/D = 0$) while it gets slightly worse in the region of $x/D > 0.3$. The HOGGDH model thus produces a better overall heat transfer rate. Although the standard value of c_θ in the GGDH model is 0.3, the use of 0.18 has been found to be the most reasonable to be coupled with the Shima model after several other test runs for channel flow cases. Consequently, the HOGGDH model is used for the TCL SMC while the GGDH model with $c_\theta = 0.18$ is used for the Shima model in the following discussions.

In Fig. 5, the predicted local *Nu* distribution at the sections of $\theta = 0°$, 45°, 90°, 135° and 180° is compared with the experiments of Johnson and Launder [2]. The levels of general agreement between the models and the experiments are fairly reasonable though some discrepancies can be found. In some regions (at $\theta = 45°$, 90° of the outer wall, etc.) the TCL SMC with the HOGGDH performs slightly better but in the other regions (at $\theta = 135°$ of the inner wall and at $\theta = 180°$ of the outer wall, etc.) the Shima model with the GGDH works slightly better. However, particularly along the outer wall of the section of $\theta = 90°$, the Shima model predicts rather high heat transfer. This is the consequence of the over-prediction of the wall normal stress in the outer region which is obvious in Fig. 3(c). The detailed discussion about the reason for this failure is addressed in the next section since this tendency is amplified in the stronger curvature case.

3.2. U-bend duct of $R_c/D = 0.65$

In the stronger curvature case, the considered bulk Reynolds number is $Re = 10^5$. Following the experiments [3,4], air flow heat transfer is considered with a constant wall heat flux boundary condition. In this case, a separating flow appears along the suction side unlike in the milder curvature case.

3.2.1. Flow field

Fig. 6 compares the predicted streamwise mean velocity distribution with the experiments of Cheah et al. [3]. Along the symmetry plane, Fig. 6(a), the TCL and the Shima models successfully reproduce the experimental distribution while the magnitude of the reverse flow at $\theta = 180°$ is slightly under-predicted. Obviously, both the models significantly improve the results of the LRN algebraic second moment closure (ASM) produced by the earlier work of Iacovides et al. [7]. Although they did not perform a full SMC, their version of the ASM

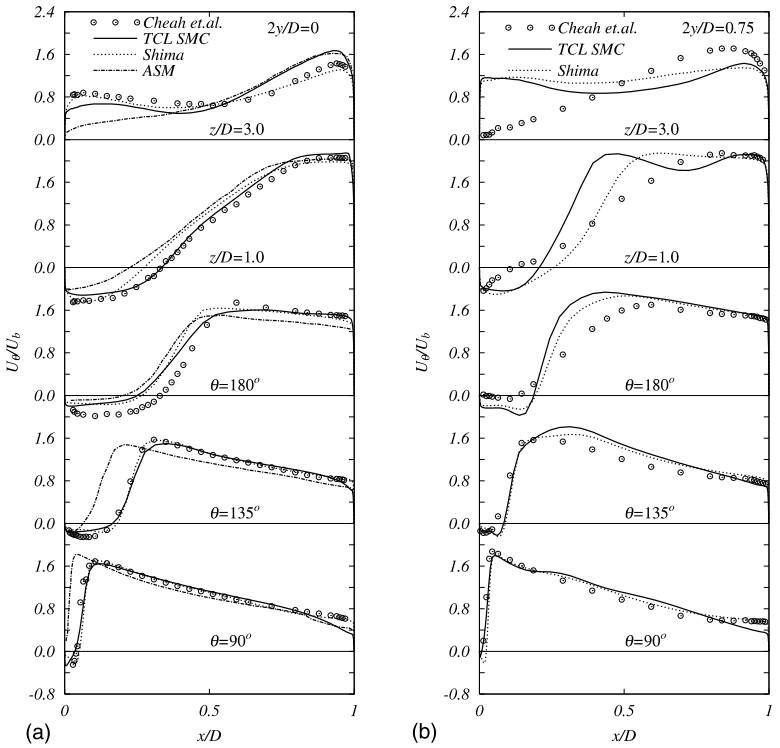

Fig. 6. Streamwise mean velocity in the U-bend duct of $R_c/D = 0.65$ at $Re = 10^5$; (a) symmetry plane ($2y/D = 0$); (b) near-wall plane ($2y/D = 0.75$).

was based on the Gibson–Launder model [24] and thus it included the wall-reflection terms. This highlights that the recently emerged wall-reflection free LRN SMCs are more reliable to predict such a complicated flow field than the earlier approach.

Along the near-wall plane of $2y/D = 0.75$, Fig. 6(b), the agreement of the TCL and the Shima models with the experiment in the inner region $(x/D < 0.5)$ of the downstream section $(z/D \geqslant 1.0)$ is somewhat poor. Although some differences can be found between the two

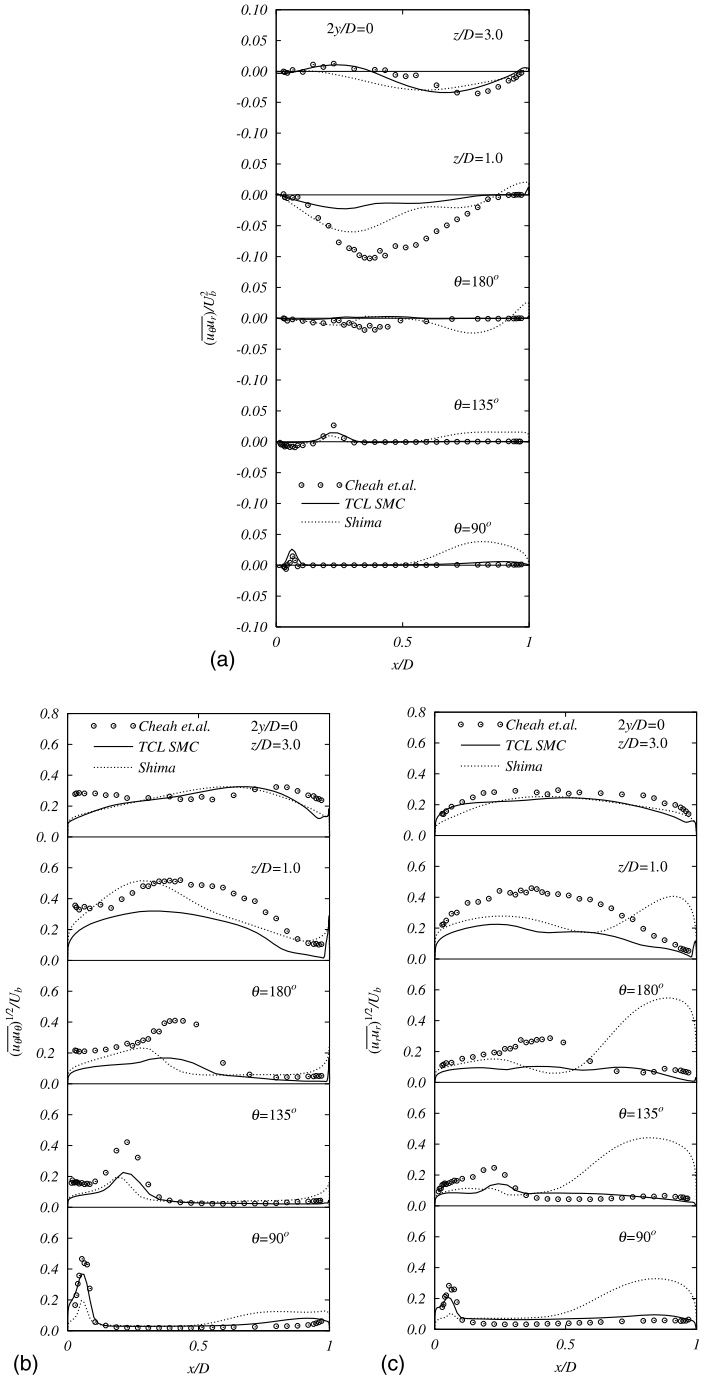

Fig. 7. Reynolds stresses along the symmetry plane of the U-bend duct of $R_c/D = 0.65$.

models, their performance in the streamwise mean velocity distribution is nearly the same.

Fig. 7 shows the distribution of Reynolds stress components along the symmetry plane. The profiles of the Reynolds shear stress: $\overline{u_\theta u_r}$ and the normal stresses: $\overline{u_\theta^2}$, $\overline{u_r^2}$ are respectively compared in Fig. 7(a)–(c). As shown in Fig. 7(a), only at the section of $z/D = 1$, the Shima model predicts better than the TCL SMC though somehow both models significantly under-predict the level of the shear stress there. At the curvature section ($90° \leqslant \theta \leqslant 180°$), the TCL SMC reasonably predicts the Reynolds shear stress while the Shima model seems to be rather unreliable in the outer region ($x/D > 0.5$). This unsatisfactory performance of the Shima model is thought to be the consequence of its wall normal stress behaviour discussed below.

As in Fig. 7(b) and (c), although the predicted peak levels of the normal stresses by the TCL SMC are rather inaccurate at the sections of $\theta = 135°$, 180° and $z/D = 1$, the results of the TCL SMC are reasonably acceptable. The Shima model performs generally similarly to the TCL SMC, but it unrealistically over-predicts the wall normal stress: $\overline{u_r^2}$ toward the outer wall in the curvature section as shown in Fig. 7(c). This tendency (though less strong) has been also pointed out in the mild curvature case. Since the Shima model was well calibrated in curvature flows [16], the reason of this puzzling behaviour needs to be understood.

Unlike fully developed curved flows, the U-bend duct flows also include effects of normal straining produced by the inertial momentum towards the outer wall due to the sharp turning. This is readily understood when one notices the increase of the magnitude of the mean velocity near the outer wall shown in Fig. 6. It is thus helpful to consider a basic normal straining flow. Fig. 8 compares the evolution of the Reynolds stresses against the normalised time: $t^* = t(S_{ij}S_{ji}/2)^{1/2}$ in an axisymmetric expansion flow of Lee and Reynolds [32]. The Shima model predicts that the Reynolds normal stresses gradually deviate from the DNS data while the TCL SMC keeps good agreement with the data. The normal strain: $\partial U/\partial x$ of the axisymmetric expansion is negative and corresponds to $\partial U_r/\partial r$ in the bend section. Thus, the behaviour of $\overline{u^2}/k$ in the axisymmetric expansion explains that the Shima model tends to predict too high normal stress: $\overline{u_r^2}$ if the normal strain is high due to the sharp turn.

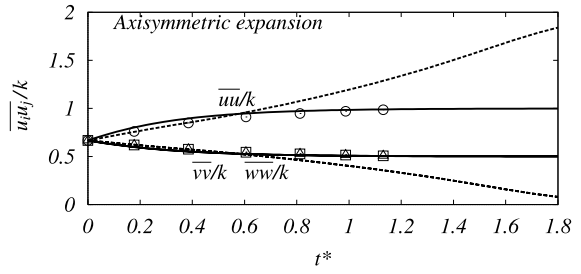

Fig. 8. Development of Reynolds stresses in the axisymmetric expansion; solid curves: TCL SMC; broken curves: Shima; symbols: DNS of Lee and Reynolds [32].

3.2.2. Heat transfer

Fig. 9 shows the predicted section-mean Nusselt number distribution compared with the experiments of Davenport [4]. Although it is not very successful, the predictive performance for the *Nu* distribution by the TCL SMC and the HOGGDH model is generally reasonable along each wall. However, the combination of the Shima model and the GGDH model shows unrealistically high level of heat transfer along the outer wall while the level is acceptable along the inner wall.

In the near-wall region, the wall normal turbulent heat flux is estimated by the GGDH model as

$$\overline{v\theta} = -c_\theta \tau \overline{v^2} \frac{\partial \Theta}{\partial y}. \tag{13}$$

This suggests that the higher the wall normal stress is predicted, the higher the predicted heat transfer becomes. Thus the unrealistically high level of the outer wall heat transfer by the Shima model is the consequence of its over-prediction of the wall normal stress.

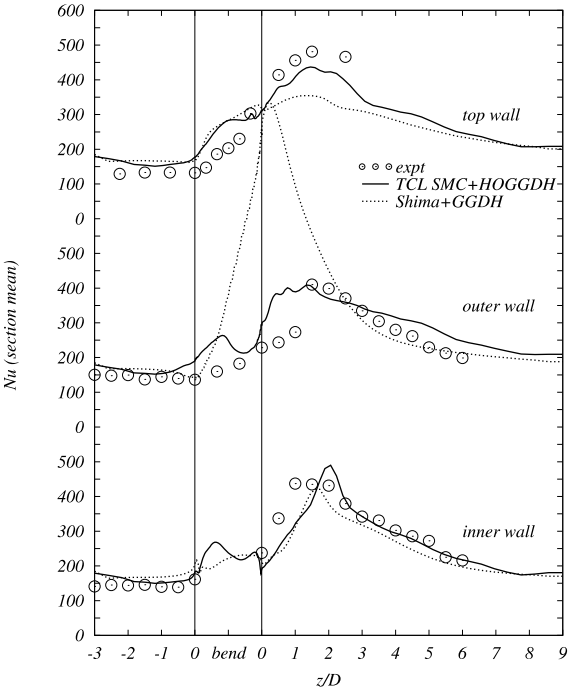

Fig. 9. Section-averaged Nusselt number distribution of the U-bend duct of $R_c/D = 0.65$ at $Re = 10^5$ and $Pr = 0.71$; expt.: Davenport [4].

(Note that to remedy this ill behaviour, the present study has also tried in vain to include an extra source term in the dissipation equation proposed by Iacovides and Raisee [33].)

4. Conclusions

In the present study, the performance of two versions of the wall-reflection free low-Reynolds-number second moment closures (the TCL SMC and the Shima model) has been validated in 3-D U-bend ducts with the mild and strong curvatures ($R_c/D = 3.357,\ 0.65$). For the turbulent heat transfer fields, the standard and the higher order GGDH heat flux models have been respectively coupled with the Shima and the TCL SMCs. The following remarks are concluded.

(1) The prediction by the TCL SMC is generally reliable for the flow fields in the U-bend ducts with both curvature ratios though some margins for improvement are still remained in the stress fields. Its overall performance is better than the one by the Shima model.
(2) The HOGGDH heat flux model produces reliable level of heat transfer in the present complicated cases when it is coupled with the TCL SMC.
(3) The Shima model performs comparably to the TCL SMC in the milder curvature case. However, in the stronger curvature case, it excessively over-predicts the wall normal stress along the outer wall, due to the strong normal straining caused by the sharp turning. This ill behaviour in the normal straining leads to the unrealistically high level of heat transfer.

Appendix A. TCL second moment closure

The model equations of the presently used modified CL model are summarised below.

As noted in Section 2.1.1 The CL model splits the pressure correlation term as

$$\Pi_{ij} = \phi_{ij} + \frac{\overline{u_i u_j}}{k}\mathrm{d}_k^{\mathrm{p}}, \tag{A.1}$$

where the second term on the rhs of the equation is regarded as a model of the pressure diffusion of $\overline{u_i u_j}$ defining the pressure diffusion of the turbulent kinetic energy as $d_k^{\mathrm{p}} = -(1/2\rho)(\partial\overline{pu_k}/\partial x_k)$. The modelled $\overline{pu_k}$ is

$$\overline{pu_k} = -\rho c_{pd}(0.5 d_k + 1.1 d_k^A)(v\varepsilon k A A_2)^{1/2}, \tag{A.2}$$

where d_i is the inhomogeneity indicator:

$$d_i = \frac{N_i}{0.5 + (N_k N_k)^{1/2}}, \quad N_i = \frac{\partial l}{\partial x_i}. \tag{A.3}$$

The present magnitude of the coefficient is slightly modified as

$$c_{pd} = 1.5(1 - A^2)[\{1 + 2\exp(-R_t/40)\}A_2 + 0.4R_t^{-1/4}\exp(-R_t/40)]. \tag{A.4}$$

The re-distributive part is modelled as Eqs. (5)–(7). For the inhomogeneity correction terms, Batten et al. [15] simplified the forms as

$$\phi_{ij1}^{\mathrm{inh}} = f_{w1}\frac{\varepsilon}{k}\left(\overline{u_l u_k}d_l^A d_k^A \delta_{ij} - \frac{3}{2}\overline{u_i u_k}d_j^A \mathrm{d}_k^A - \frac{3}{2}\overline{u_j u_k}d_i^A d_k^A\right) + f_{w2}\frac{\varepsilon}{k^2}\left(\overline{u_m u_n}\,\overline{u_m u_l}d_n^A d_l^A \delta_{ij} - \frac{3}{2}\overline{u_i u_m}\,\overline{u_m u_l}d_j^A d_l^A - \frac{3}{2}\overline{u_j u_m}\,\overline{u_m u_l}d_i^A d_l^A\right), \tag{A.5}$$

$$\phi_{ij2}^{\mathrm{inh}} = f_I k\frac{\partial U_l}{\partial x_n}d_l d_n\left(d_i d_j - \frac{1}{3}d_k d_k \delta_{ij}\right) \tag{A.6}$$

with

$$d_i^A = \frac{N_i^A}{0.5 + (N_k^A N_k^A)^{1/2}}, \quad N_i^A = \frac{\partial(lA^{1/2})}{\partial x_i}. \tag{A.7}$$

The presently used coefficients are mostly followed Batten et al. [15], but some are slightly re-tuned as in Table 1 to balance with the change for the compliance of the behaviour of A with the theoretical one.

For the turbulent diffusion process, although the original CL model employs an ASM procedure for the

Table 1
Model coefficients and functions in the TCL second moment closure

$c_1 = 3.2 f_A\sqrt{A_2} f_{Rt}$	$c_2 = \min\left[0.55\left\{1 - \exp\left(\frac{-A^{3/2}R_t}{100}\right)\right\}, \frac{3.2A}{1+S}\right]$	$c_1' = 1.1$	$c_2' = \min(0.6, \sqrt{A}) + f_S$
$f_{w1} = 3(1-\sqrt{A})f_{R_t}'$	$f_{w2} = 0.6A_2(1-\sqrt{A})f_{R_t}'' + 0.1$	$c_1'' = A^{1/2}$	$f_{R_t} = \min\left\{\left(\frac{R_t}{200}\right)^2, 1\right\}$
$f_A = \sqrt{A/14},\ A \leqslant 0.05$	$f_{R_t}' = \min\left\{1, \max\left(0, 1 - \frac{R_t - 55}{70}\right)\right\}$	$f_I = 3f_A$	$f_{R_t}'' = \min\left\{1, \max\left(0, 1 - \frac{R_t - 50}{200}\right)\right\}$
$= A/\sqrt{0.7},\ 0.05 < A < 0.7$	$f_R = (1-A)\min\{(R_t/80)^2, 1\}$		$f_\epsilon = 20A^{3/2},\ A \leqslant 0.05$
$= \sqrt{A},\ A \geqslant 0.7$	$f_S = \frac{3.5(S-\Omega)}{3+S+\Omega} - 4\sqrt{6}\min(S_I, 0)$		$= \sqrt{A},\ A > 0.05$

triple moments, Batten et al. returned to the usual GGDH model of Daly and Harlow [17]:

$$d_{ij} = \frac{\partial}{\partial x_k}\left\{\left(\nu\delta_{kl} + 0.22\overline{u_k u_l}\frac{k}{\varepsilon}\right)\frac{\partial \overline{u_i u_j}}{\partial x_l}\right\}. \tag{A.8}$$

The dissipation tensor is modelled as

$$\varepsilon_{ij} = (1 - f_\varepsilon)(\varepsilon'_{ij} + \varepsilon''_{ij})/D + \tfrac{2}{3}\delta_{ij} f_\varepsilon \varepsilon \tag{A.9}$$

with

$$\varepsilon'_{ij} = 2\nu\frac{\partial\sqrt{k}}{\partial x_m}\left(\frac{\partial\sqrt{k}}{\partial x_i}\frac{\overline{u_j u_m}}{k} + \frac{\partial\sqrt{k}}{\partial x_j}\frac{\overline{u_i u_m}}{k}\right) + 2\nu\frac{\partial\sqrt{k}}{\partial x_k}\frac{\partial\sqrt{k}}{\partial x_m}\frac{\overline{u_k u_m}}{k}\delta_{ij} + \frac{\overline{u_i u_j}}{k}\varepsilon, \tag{A.10}$$

$$\varepsilon''_{ij} = f_R\varepsilon\left(2\frac{\overline{u_l u_k}}{k}d_l^A d_k^A\delta_{ij} - \frac{\overline{u_i u_l}}{k}d_l^A d_j^A - \frac{\overline{u_j u_l}}{k}d_l^A d_i^A\right), \tag{A.11}$$

where $D = (\varepsilon'_{kk} + \varepsilon''_{kk})/(2\varepsilon)$. Batten et al.'s modified version uses $f_\varepsilon = \sqrt{A}$, however it does not lead to the correct near-wall limiting behaviour of $\varepsilon_{22}(\propto y^{+2})$. The present study has experienced that this is important to obtain the correct near-wall behaviour of $A(\propto y^{+2})$ which is expected in some model functions. The present study thus modifies it as

$$f_\varepsilon = 20A^{1.5}(A \leqslant 0.05) = \sqrt{A}(A > 0.05). \tag{A.12}$$

The transport equation for the isotropic dissipation rate $\tilde{\varepsilon}$ is modelled as

$$\frac{D\tilde{\varepsilon}}{Dt} = \frac{\partial}{\partial x_k}\left\{\left(\nu\delta_{kl} + 0.18\overline{u_k u_l}\frac{k}{\varepsilon}\right)\frac{\partial\tilde{\varepsilon}}{\partial x_l}\right\} + c_{\varepsilon 1}\frac{P_{kk}}{2}\frac{\tilde{\varepsilon}}{k} - c_{\varepsilon 2}\frac{\tilde{\varepsilon}^2}{k} - \frac{(\varepsilon - \tilde{\varepsilon})\tilde{\varepsilon}}{k} + P_{\varepsilon 3} + Y_E, \tag{A.13}$$

where $c_{\varepsilon 1} = 1.0$, $c_{\varepsilon 2} = 1.92/(1 + 0.7AA_d^{1/2})$, $A_d = \min(A_2, 0.4)$ and

$$P_{\varepsilon 3} = 0.7\nu\overline{u_i u_j}\frac{k}{\varepsilon}\frac{\partial^2 U_k}{\partial x_i \partial x_l}\frac{\partial^2 U_k}{\partial x_j \partial x_l}. \tag{A.14}$$

The length-scale correction term of Iacovides and Raisee [33]:

$$Y_E = 0.83\frac{\tilde{\varepsilon}^2}{k}\max\{F(F+1)^2, 0\} \tag{A.15}$$

is employed with

$$F = \frac{1}{c_l}\left(\frac{\partial l}{\partial x_j}\frac{\partial l}{\partial x_j}\right)^{1/2} - \{1 - \exp(-B_\varepsilon R_t) + B_\varepsilon R_t\exp(-B_\varepsilon R_t)\}, \tag{A.16}$$

$c_l = 2.55$ and $B_\varepsilon = 0.1069$.

References

[1] S.M. Chang, J.A.C. Humphrey, A. Modavi, Turbulent flow in a strongly curved U-bend and downstream tangent of square cross-sections, Phys. Chem. Hydrodyn. 4 (3) (1983) 243–269.

[2] R.W. Johnson, B.E. Launder, Local Nusselt number and temperature field in turbulent flow through a heated square-sectioned U-bend, Int. J. Heat Fluid Flow 6 (3) (1985) 171–180.

[3] S.C. Cheah, H. Iacovides, D.C. Jackson, H. Ji, B.E. Launder, LDA investigation of the flow development through rotating U-ducts, Trans. ASME J. Turbomach. 118 (1996) 590–596.

[4] R. Davenport, Innovative use of thermochronic liquid crystals for turbine-blade cooling passage flow visualization and heat transfer measurements, in: Proceedings of European Propulsion Forum, Modern Techniques and Developments in Engine and Component Testing, Bath, UK, 1989.

[5] T. Bo, H. Iacovides, B.E. Launder, Convective discretization schemes for the turbulence transport equations in flow predictions through sharp U-bends, Int. J. Num. Meth. Heat Fluid Flow 5 (1995) 33–48.

[6] H. Iacovides, B.E. Launder, H.Y. Li, Application of a reflection free DSM to turbulent flow and heat transfer in a square-sectioned U-bend, Exper. Therm. Fluid Sci. 13 (1996) 419–429.

[7] H. Iacovides, B.E. Launder, H.-Y. Li, The computation of flow development through stationary and rotating U-ducts of strong curvature, Int. J. Heat Fluid Flow 17 (1) (1996) 22–33.

[8] H. Iacovides, B.E. Launder, Computational fluid dynamics applied to internal gas-turbine blade cooling: a review, Int. J. Heat Fluid Flow 16 (6) (1995) 454–470.

[9] B.E. Launder, D.P. Tselepidakis, Contribution to the modelling of near-wall turbulence, in: F. Durst, et al. (Eds.), Turbulent Shear Flows, vol. 8, Springer, Berlin, 1993, pp. 81–96.

[10] K. Hanjalić, S. Jakirlić, A model of stress dissipation in second moment closures, in: F.T. Nieuwstadt (Ed.), Advances in Turbulence IV, Applied Scientific Research, vol. 51, Kluwer, Dordrecht, 1993, pp. 513–518.

[11] T.J. Craft, B.E. Launder, A Reynolds-stress closure designed for complex geometries, Int. J. Heat Fluid Flow 17 (1996) 245–254.

[12] N. Shima, Low-Reynolds-number second-moment closure without wall-reflection redistribution terms, Int. J. Heat Fluid Flow 19 (1998) 549–555.

[13] B.E. Launder, S.-P. Li, On the elimination of wall-topography parameters from second-moment closure, Phys. Fluids 6 (2) (1994) 999–1006.

[14] S. Fu, Computational modelling of turbulent swirling flows with second-moment closures, Ph.D. Thesis, Faculty of Technology, University of Manchester, 1988.

[15] P. Batten, T.J. Craft, M.A. Leschziner, H. Loyau, Reynolds-stress-transport modeling for compressible aerodynamics applications, AIAA J. 37 (7) (1999) 785–797.

[16] N. Shima, T. Kawai, M. Okamoto, R. Tsuchikura, Prediction of streamline curvature effects on wall-bounded turbulent flows, Int. J. Heat Fluid Flow 21 (2000) 614–619.

[17] B.J. Daly, F.H. Harlow, Transport equation in turbulence, Phys. Fluids 13 (1970) 2634–2649.
[18] B.E. Launder, On the computation of convective heat transfer in complex turbulent flows, ASME J. Heat Transfer 110 (1988) 1112–1128.
[19] M.M. Rogers, N.N. Mansour, W.C. Reynolds, An algebraic model for the turbulent flux of a passive scalar, J. Fluid Mech. 203 (1989) 77–101.
[20] R.M.C. So, T.P. Sommer, An explicit algebraic heat-flux model for the temperature field, Int. J. Heat Mass Transfer 39 (3) (1996) 455–465.
[21] K. Suga, K. Abe, Nonlinear eddy viscosity modelling for turbulence and heat transfer near wall and shear-free boundaries, Int. J. Heat Fluid Flow 21 (1) (2000) 37–48.
[22] B.E. Launder, G.J. Reece, W. Rodi, Progress in the development of a Reynolds stress turbulence closure, J. Fluid Mech. 68 (1975) 537–566.
[23] C.G. Speziale, S. Sarkar, T.B. Gatski, Modelling the pressure-strain correlation of turbulence: an invariant dynamical systems approach, J. Fluid Mech. 227 (1991) 245–272.
[24] M.M. Gibson, B.E. Launder, Ground effects on pressure fluctuations in the atmospheric boundary layer, J. Fluid Mech. 86 (1978) 491–511.
[25] B.E. Launder, N. Shima, Second-moment closure for the near-wall sublayer: development and application, AIAA J. 27 (1989) 1319–1325.
[26] J.L. Lumley, Computational modeling of turbulent flows, Adv. Appl. Mech. 18 (1978) 123–176.
[27] K. Abe, K. Suga, Toward the development of a Reynolds-averaged algebraic turbulent scalar-flux model, Int. J. Heat Fluid Flow 22 (1) (2001) 19–29.
[28] S. Pope, Consistent modelling of scalars in turbulent flows, Phys. Fluids 26 (2) (1983) 404–408.
[29] K. Suga, M. Nagaoka, N. Horinouchi, K. Abe, Y. Kondo, Application of a three equation cubic eddy viscosity model to 3-D turbulent flows by the unstructured grid method, Int. J. Heat Fluid Flow 22 (3) (2001) 259–271.
[30] Y.D. Choi, C. Moon, S.H. Yang, Measurement of turbulent flow characteristics of square duct with a 180° bend by hot wire anemometer, in: Proceedings of International Symposium on Engineering Turbulence Modelling and Measurements, Dubrovnik, Yugoslavia, 1990, pp. 429–438.
[31] N. Fukushima, N. Kasagi, The effect of walls on turbulent flow and temperature fields, in: Proceedings of Turbulent Heat Transfer III, Anchorage, USA, 2001.
[32] M.J. Lee, W.C. Reynolds, Numerical experiments on the structure of homogeneous turbulence, Stanford Univ. Tech. Rep. TF-24 (1985).
[33] H. Iacovides, M. Raisee, Recent progress in the computation of flow and heat transfer in internal cooling passages of turbine blades, Int. J. Heat Fluid Flow 20 (1999) 320–328.